# 7 Mean-Field Theory of Spin and Charge Order in the Two-Dimensional Hubbard Model

Walter Metzner
Max Planck Institute for Solid State Research
D-70569 Stuttgart, Germany

## Contents



E. Pavarini and E. Koch (eds.)
Correlated Materials: Methods and Applications
Modeling and Simulation Vol. 16, Forschungszentrum Jülich, 2026
ISBN 978-3-95806-909-1 http://www.cond-mat.de/events/correl26

# 1 Introduction

The two-dimensional Hubbard model is a prototype for competing ordering tendencies in interacting electron systems. It captures key features of the valence electrons in high-$T_c$ cuprates such as antiferromagnetism and $d$-wave superconductivity [1]. In spite of substantial progress in the development of quantum many body methods, only fragments of the phase diagram of this important model have been firmly established [2, 3].

There is no doubt that at half-filling the ground state of the two-dimensional Hubbard model with pure nearest neighbor hopping is a Néel ordered antiferromagnet for any repulsive Hubbard interaction $U > 0$, and beyond a certain critical repulsion if hopping amplitudes beyond nearest neighbors are present. However, for electron densities away from half-filling, the Néel state easily becomes unstable [4–7], leading to other magnetic states or possibly phase separation. Moreover, the Hubbard model away from half-filling is usually metallic and thus prone to pairing instabilities.

There is a whole zoo of possible magnetic states. Unlike the Néel state, most of them are characterized by one or several ordering wave vectors which are generically incommensurate with the lattice periodicity. Many approximate calculations point toward planar circular spirals [4–16] and collinear spin density waves [17–25] as the most important candidates. The latter entail charge order with regions of reduced charge density arranged along one-dimensional lines, and are therefore also known as "spin-charge stripes" [26]. By contrast, the charge distribution of circular spiral states remains uniform.

Recently, exact numerical calculations on finite lattices have provided strong evidence for stripe order in the ground state of the Hubbard model with pure nearest neighbor hopping and large $U$ for special hole-doping fractions: $1/10$ and $1/8$, corresponding to electron densities $0.9$ and $0.875$, respectively [27,28]. No superconductivity was found in these cases. However, allowing for next-nearest neighbor hopping, superconductivity reemerges for a range of densities away from half-filling [29]. Exact numerical evaluations at finite temperatures yield peaks in the spin susceptibility at the Néel wave vector $(\pi, \pi)$ near half-filling, and peaks at incommensurate wave vectors in the spin and charge susceptibility for sufficiently large doping [30, 31].

Unlike superconductivity, magnetic order in the (repulsive) Hubbard model can be captured already within a static mean-field approximation, also known as Hartree-Fock theory. While the size of the order parameter and the regime of ordered states in the phase diagram are grossly overestimated by mean-field theory, finite size effects can be studied in more detail because much larger lattices can be dealt with. For Néel, circular spiral, and stripe states, mean-field calculations can be performed directly in the thermodynamic limit, albeit only for wave vectors commensurate with the lattice in the case of stripes. Indeed, numerous Hartree-Fock studies of the two-dimensional Hubbard model have been carried out. However, in many of them the magnetic states were restricted to ferromagnetic and Néel [32–34], or spiral order [12]. The latter includes ferromagnetic and Néel states as the special cases with wave vectors $(0, 0)$ and $(\pi, \pi)$, respectively. For small hole doping, this restriction often leads to phase separation in paramagnetic, ferromagnetic, and antiferromagnetic regions [12, 34]. Allowing for arbitrary

collinear spin order or even for completely arbitrary spin configurations – combined with charge order – spin-charge stripes have been found [17–21].
At finite temperatures, magnetic long-range order in two-dimensional systems with SU(2) spin symmetry is prohibited by thermal fluctuations, as is rigorously established by the Mermin-Wagner theorem [35]. Magnetic states obtained in Hartree-Fock approximation at finite temperatures obviously violate this theorem. However, such states become meaningful as an ingredient for theories of fluctuating magnetic order, where the electron is fractionalized into a "chargon" with a magnetically ordered pseudospin, and a fluctuating spin rotation matrix, which conserves the SU(2) spin symmetry of the electronic state [36–38].
A comprehensive and completely unrestricted Hartree-Fock study of the two-dimensional Hubbard model at zero and finite temperatures has been performed only recently [39, 40]. Unrestricted real space calculations on large lattices (from $20\times20$ to $48\times48$) have been complemented by momentum space calculations for Néel, spiral, and commensurate stripe states in the thermodynamic limit. In this lecture I describe the various approaches for solving the Hartree-Fock equations, and I review the results for the two-dimensional Hubbard model with a moderate interaction strength, in particular its magnetic phase diagram as a function of density and temperature. Both the "pure" Hubbard model, with pure nearest neighbor hopping $t$, as well as its physically more relevant extension with a next-nearest neighbor hopping $t'$ will be considered.

# 2 Unrestricted Hartree-Fock theory

## 2.1 Hubbard model

The Hubbard Hamiltonian for spin-$\frac{1}{2}$ fermions with intersite hopping amplitudes $t_{jj'}$ and a local interaction $U$ reads

$$H = H_0 + H_{\text{int}} = \sum_{j,j',\sigma} t_{jj'} c^\dagger_{j\sigma} c_{j'\sigma} + U \sum_j n_{j\uparrow} n_{j\downarrow} \,, \tag{1}$$

where $c_{j\sigma}$ ($c^\dagger_{j\sigma}$) annihilates (creates) an electron on lattice site $j$ with spin orientation $\sigma$ ($\uparrow$ or $\downarrow$), and $n_{j\sigma} = c^\dagger_{j\sigma} c_{j\sigma}$. We consider exclusively the Hubbard model on a square lattice. The hopping matrix $t_{jj'}$ depends only on the distance between the sites $j$ and $j'$. We restrict it to nearest neighbor contributions with an amplitude $-t$, and to next-nearest neighbor contributions with an amplitude $-t'$. The bare dispersion relation is then given by

$$\varepsilon_{\mathbf{k}} = -2t\big(\cos k_x + \cos k_y\big) - 4t' \cos k_x \cos k_y \,. \tag{2}$$

We focus on the repulsive Hubbard model where $U$ is positive, corresponding to a screened Coulomb repulsion between electrons. The repulsive two-dimensional Hubbard model is the most intensively studied model for the electrons moving in the copper-oxide planes of cuprate high temperature superconductors [1]. We use the nearest neighbor hopping amplitude $t$ as our energy unit, that is, we set $t = 1$ in numerical results.

## 2.2 Hartree-Fock equations in real space

In the mean-field (Hartree-Fock) approximation, the interaction part of the Hamiltonian $H_{\text{int}}$ is replaced by effective quadratic (in $c$, $c^\dagger$) terms. Following Zaanen and Gunnarsson [18], we decouple $H_{\text{int}}$ as

$$H_{\text{int}}^{\text{MF}} = \sum_{j\sigma} \Delta_{j\bar{\sigma}} n_{j\sigma} - \sum_j \left( \Delta_{j-} c_{j\uparrow}^\dagger c_{j\downarrow} + \Delta_{j+} c_{j\downarrow}^\dagger c_{j\uparrow} \right) - \frac{1}{U} \sum_j \left( \Delta_{j\uparrow} \Delta_{j\downarrow} - \Delta_{j-} \Delta_{j+} \right), \tag{3}$$

with the convention $\overline{\uparrow} = \downarrow$ and $\overline{\downarrow} = \uparrow$. The parameters $\Delta_{j\alpha}$ are self-consistently determined by the "gap equations"

$$\Delta_{j\sigma} = U \langle n_{j\sigma} \rangle, \tag{4a}$$

$$\Delta_{j+} = \Delta_{j-}^* = U \langle c_{j\uparrow}^\dagger c_{j\downarrow} \rangle. \tag{4b}$$

The decoupling in Eq. (3) allows for arbitrary spin and charge patterns. In most of the previous mean-field studies of the Hubbard model, only the first (Hartree) or the second (Fock) term on the right hand side of Eq. (3) has been considered, restricting the spin order to collinear or spiral order, respectively.

The mean-field equations can be solved iteratively on finite lattices. We denote the total number of lattice sites by $L = L_x L_y$, where $L_x$ and $L_y$ is the number of sites in $x$ and $y$ direction, respectively. The mean-field Hamiltonian can be written in matrix form as

$$H^{\text{MF}} = H_0 + H_{\text{int}}^{\text{MF}} = \sum_{j,j'} \sum_{\sigma,\sigma'} c_{j\sigma}^\dagger \mathcal{H}_{jj'}^{\sigma\sigma'} c_{j'\sigma'} + \text{const.}\,, \tag{5}$$

where $\mathcal{H}_{jj'}^{\sigma\sigma'} \in \mathbb{C}^{2L\times 2L}$ is a square matrix with $4L$ real parameters to be determined self-consistently ($\Delta_{j\uparrow}$, $\Delta_{j\downarrow}$, $\mathrm{Re}\,\Delta_{j+}$, and $\mathrm{Im}\,\Delta_{j+}$ for each lattice site). These parameters are related to the expectation values of the charge and spin order parameters by

$$\Delta_{j\uparrow} + \Delta_{j\downarrow} = U \langle n_j \rangle\,, \tag{6a}$$

$$\Delta_{j\uparrow} - \Delta_{j\downarrow} = 2U \langle S_j^z \rangle\,, \tag{6b}$$

$$\Delta_{j+} + \Delta_{j-} = 2U \langle S_j^x \rangle\,, \tag{6c}$$

$$\Delta_{j+} - \Delta_{j-} = 2iU \langle S_j^y \rangle\,, \tag{6d}$$

where $n_j = n_{j\uparrow} + n_{j\downarrow}$ and $\vec{S}_j = \frac{1}{2} c_j^\dagger \vec{\sigma} c_j$, with the Pauli matrices $\vec{\sigma} = (\sigma^x, \sigma^y, \sigma^z)$.

The calculations can be preformed at fixed density $n$ by enforcing the constraint $L^{-1} \sum_{j\sigma} \langle n_{j\sigma} \rangle = n$. In the ground state this is achieved by calculating the expectation values on the right-hand side of Eq. (4) as

$$\left\langle c_{j\sigma}^\dagger c_{j\sigma'} \right\rangle = \sum_{\ell=1}^{N} (v_{j\sigma}^\ell)^* v_{j\sigma'}^\ell, \tag{7}$$

where $N$ is the total particle number, $\ell$ labels the $2L$ eigenvalues $\varepsilon_\ell$ of $\mathcal{H}_{jj'}^{\sigma\sigma'}$ in ascending order, and $v_{j\sigma}^\ell$ is the normalized eigenvector corresponding to the $\ell$-th eigenvalue. At finite temperatures $T > 0$, one needs to introduce a chemical potential $\mu$, and Eq. (7) is replaced by

$$\left\langle c_{j\sigma}^\dagger c_{j\sigma'} \right\rangle = \sum_{\ell=1}^{2L} (v_{j\sigma}^\ell)^* v_{j\sigma'}^\ell f(\varepsilon_\ell - \mu), \tag{8}$$

with $f(\varepsilon) = 1/(1+e^{\varepsilon/T})$ the Fermi distribution function. The chemical potential is adjusted to enforce the chosen value for the average density

$$L^{-1}\sum_j \langle n_j\rangle = L^{-1}\sum_{\ell=1}^{2L} f(\varepsilon_\ell - \mu) = n. \tag{9}$$

This relation is obtained via the orthonormality property of the eigenvectors $\sum_{j,\sigma}(v_{j\sigma}^\ell)^* v_{j\sigma}^\ell = 1$. The system of mean-field equations can be solved in the following iterative manner: A random initial set of parameters $\Delta_{j\alpha}$ with $\alpha \in \{\uparrow,\downarrow,+,-\}$ and $\Delta_{j-} = \Delta_{j+}^*$, is plugged into $\mathcal{H}_{jj'}^{\sigma\sigma'}$, from which the eigenvectors and the expectation values in Eq. (4) are computed to update the values of $\Delta_{j\alpha}$. This procedure is repeated until convergence is reached. At finite temperatures, the chemical potential is computed at every iteration from Eq. (9).
Within the mean-field approximation, the free energy is given by

$$F = -T\sum_\ell \log\left[1+e^{-\beta(\varepsilon_\ell-\mu)}\right] - \frac{1}{U}\sum_j\left(\Delta_{j\uparrow}\Delta_{j\downarrow} - \Delta_{j-}\Delta_{j+}\right) + \mu N. \tag{10}$$

## 2.3 Classification of magnetic states

The zoo of distinct magnetic states obtained from the unrestricted mean-field calculations can be classified solely according to their spin pattern [41]. The modulation of the charge density is roughly proportional to the square of the spin amplitudes, that is,

$$\langle n_j\rangle \approx \text{const.}\,\langle \vec{S}_j^2\rangle + \text{const.}, \tag{11}$$

as can be deduced from the lowest order coupling between the charge and spin density wave order parameters in a Landau theory [42].
To identify a state from a (converged) real space spin pattern defined by the spin expectation values $\langle\vec{S}_j\rangle$, it is convenient to use a Fourier representation,

$$\langle\vec{S}_j\rangle = \sum_{\mathbf{q}} \vec{\mathcal{S}}_{\mathbf{q}}\, e^{i\mathbf{q}\cdot\mathbf{r}_j}, \tag{12}$$

where $\vec{\mathcal{S}}_{\mathbf{q}}$ with $\vec{\mathcal{S}}_{\mathbf{q}} = \vec{\mathcal{S}}_{-\mathbf{q}}^*$ is the Fourier component of the spins with wave vector $\mathbf{q}$, and $\mathbf{r}_j$ represents the real space coordinate of lattice site $j$. The sum runs over the $L = L_xL_y$ momenta allowed by the periodic boundary conditions on the finite lattice. Restricting $L_x$ and $L_y$ to even numbers, the allowed momenta can be written as

$$\mathbf{q} \in \left\{ (\pi - 2\pi\nu_x/L_x,\, \pi - 2\pi\nu_y/L_y) \,\middle|\, \nu_\alpha \in \{0,1,\ldots,L_\alpha - 1\}\right\}. \tag{13}$$

In the majority of cases only one or two modes with fixed wave vectors $\mathbf{q}$ (together with their partner $-\mathbf{q}$) contribute significantly to $\langle\vec{S}_j\rangle$. Usually, these wave vectors have the form $\mathbf{Q}_x = (\pi - 2\pi\eta_x, \pi)$ and/or $\mathbf{Q}_y = (\pi, \pi - 2\pi\eta_y)$. The parameters $\eta_\alpha$ are frequently referred to as "incommensurabilities" in the literature. In a finite system, $\eta_\alpha$ is restricted to integer multiples of $1/L_\alpha$. For lattices with $L_x = L_y$, one always finds $\eta_x = \eta_y \equiv \eta$. States with diagonal wave

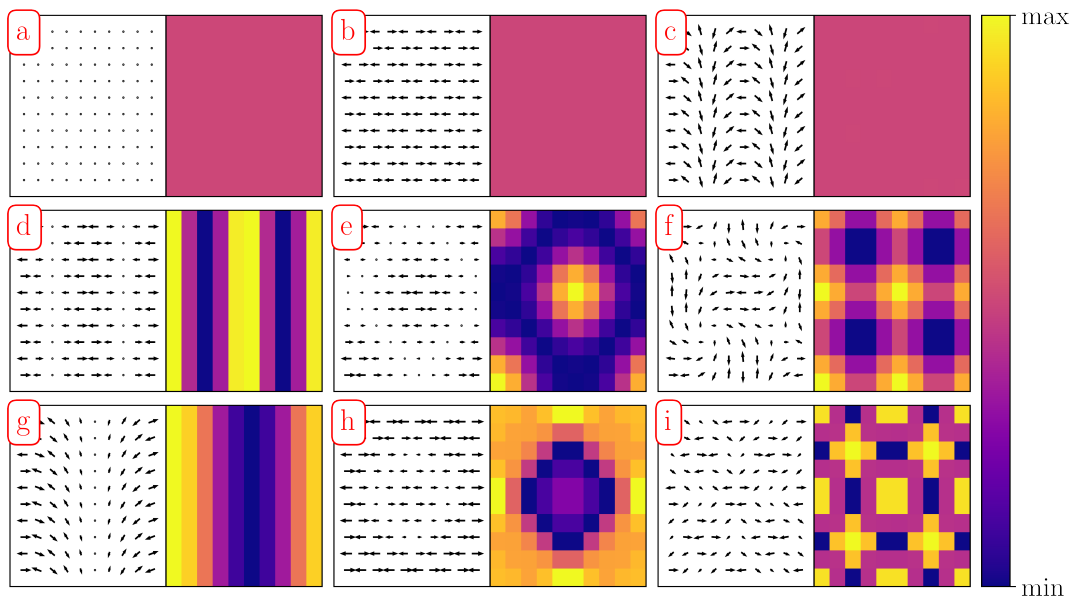


**Fig. 1:** *Distinct orders found in unrestricted mean-field calculations, schematically shown on a* $10\times10$ *lattice. In each panel, the square on the left shows the relative spin orientations and amplitudes (length of the arrows) of each phase, choosing a frame such that the spins lie in the* $xy$ *plane and the bottom left spin points along the* $x$ *direction. The right plot in each panel shows the corresponding charge modulation, using a color code defined on the right edge of the figure. The various panels exemplify the following magnetic orders: (a) paramagnetism, (b) Néel antiferromagnetism, (c) spiral order, (d) stripe order, (e) collinear bidirectional stripe order, (f) coplanar bidirectional stripe order, (g) beat order, (h) other collinear orders, (i) "strange" order. Only one example of strange order is shown.*

vectors of the form $\mathbf{Q}_{xy} \equiv (\pi - 2\pi\eta,\ \pi - 2\pi\eta)$ as dominant contributions are rarely found, and typically only for relatively small lattices.
In cases with only one mode, one can express $\vec{\mathcal{S}}_{\mathbf{q}}$ as

$$\vec{\mathcal{S}}_{\mathbf{q}} = \frac{1}{2}\left(\vec{\mathcal{S}}\,\delta_{\mathbf{q},\mathbf{Q}} + \vec{\mathcal{S}}^{*}\,\delta_{\mathbf{q},-\mathbf{Q}}\right), \tag{14}$$

where $\mathbf{Q}$ has the form $\mathbf{Q}_x$ or $\mathbf{Q}_y$. In states with two modes, one has

$$\vec{\mathcal{S}}_{\mathbf{q}} = \frac{1}{2}\left(\vec{\mathcal{S}}_x\,\delta_{\mathbf{q},\mathbf{Q}_x} + \vec{\mathcal{S}}_x^{*}\,\delta_{\mathbf{q},-\mathbf{Q}_x}\right) + \frac{1}{2}\left(\vec{\mathcal{S}}_y\,\delta_{\mathbf{q},\mathbf{Q}_y} + \vec{\mathcal{S}}_y^{*}\,\delta_{\mathbf{q},-\mathbf{Q}_y}\right). \tag{15}$$

Depending on the model parameters, temperature, and lattice size, the unrestricted mean-field calculations yield 9 distinct states [39]. The spin and charge order pattern for a representative of each state is sketched in Fig. 1. States that can be transformed into each other by a point group symmetry operation of the lattice (rotations and reflections), by a spatial translation (changing the phases of $\vec{\mathcal{S}}_x$ and $\vec{\mathcal{S}}_y$), or by a global SU(2) rotation of the spin frame, belong to the same class. In the following, each class is described by one of its representatives. In principle, there might be other possible spin configurations, for example the phases $F$ and $G$ in the classification of Ref. [41], but they never appear in the fairly broad parameter regime explored in Ref. [39].

### 2.3.1 Paramagnetism

In the paramagnetic phase the expectation value of the spin on each site vanishes, i.e., $\langle \vec{S}_j \rangle = \vec{0}$, and the charge distribution is uniform, $\langle n_j \rangle = n$ (see panel (a) of Fig. 1).

### 2.3.2 Néel antiferromagnetism

In a Néel antiferromagnet only $\vec{\mathcal{S}}_{(\pi,\pi)}$ is nonzero. In real space, adjacent spins point in opposite directions, all spins have the same amplitude, and the charge is homogeneously distributed, as shown in panel (b) of Fig. 1.

### 2.3.3 Spiral

Planar circular spiral states are briefly referred to as "spiral" states. Such a state is characterized by a single mode with a wave vector $\mathbf{Q}$, and (as a representative)

$$\vec{\mathcal{S}} = S_0 \begin{pmatrix} 1 \\ i \\ 0 \end{pmatrix}, \tag{16}$$

where $S_0$ is a real number. In real space, the corresponding spin pattern has the form

$$\langle \vec{S}_j \rangle = S_0 \begin{pmatrix} \cos(\mathbf{Q}\cdot\mathbf{r}_j) \\ \sin(\mathbf{Q}\cdot\mathbf{r}_j) \\ 0 \end{pmatrix}. \tag{17}$$

The spin magnitude $|\langle \vec{S}_j \rangle|$ is constant (independent of site $j$), and the charge distribution is therefore homogeneous, as shown in panel (c) of Fig. 1. The wave vector $\mathbf{Q}$ has the form $\mathbf{Q}_x = (\pi{-}2\pi\eta,\, \pi)$ or $\mathbf{Q}_y = (\pi,\, \pi{-}2\pi\eta)$, that is, only one component deviates from $\pi$. The Néel state can be viewed as the special case of a spiral with $\mathbf{Q} = (\pi, \pi)$.

### 2.3.4 Collinear unidirectional stripes

Stripe states are generally a superposition of several Fourier modes. However, usually one of them is much larger than all others. For a collinear unidirectional stripe state described by a single $\mathbf{q}$-mode, the amplitude has the form

$$\vec{\mathcal{S}} = S_0 \begin{pmatrix} 1 \\ 0 \\ 0 \end{pmatrix}. \tag{18}$$

In this state the spins are ordered collinearly, and the spin modulation in real space is given by

$$\langle \vec{S}_j \rangle = S_0 \begin{pmatrix} \cos(\mathbf{Q}\cdot\mathbf{r}_j) \\ 0 \\ 0 \end{pmatrix}. \tag{19}$$

Once again, the wave vector $\mathbf{Q}$ has either the form $\mathbf{Q}_x$ or $\mathbf{Q}_y$. The charge order of this state is a unidirectional charge density wave with a wave vector $2\mathbf{Q}$, that is, $\langle n_j \rangle - n \propto \cos(2\mathbf{Q}\cdot\mathbf{r}_j)$. The minima in the amplitude of the spin coincide with the minima of the charge modulation, as shown in panel (d) of Fig. 1.

### 2.3.5 Collinear bidirectional stripes (ClBS)

A collinear bidirectional stripe consists of two orthogonal stripes with parallel spin orientations, that is, the (dominant) components of $\vec{\mathcal{S}}_{\mathbf{q}}$ in Eq. (15) are given by

$$\vec{\mathcal{S}}_x = \vec{\mathcal{S}}_y = S_0 \begin{pmatrix} 1 \\ 0 \\ 0 \end{pmatrix}, \tag{20}$$

where $S_0$ is a real constant. In real space, this corresponds to

$$\langle \vec{S}_j \rangle = S_0 \begin{pmatrix} \cos(\mathbf{Q}_x\cdot\mathbf{r}_j) + \cos(\mathbf{Q}_y\cdot\mathbf{r}_j) \\ 0 \\ 0 \end{pmatrix}. \tag{21}$$

This phase has charge modulations in both $x$ and $y$ directions, proportional to $\big[\cos(\mathbf{Q}_x\cdot\mathbf{r}_j) + \cos(\mathbf{Q}_y\cdot\mathbf{r}_j)\big]^2$, as displayed in panel (e) of Fig. 1.

### 2.3.6 Coplanar bidirectional stripes (CpBS)

A coplanar bidirectional stripe state consists of two orthogonal stripes with orthogonal spin orientations, that is, with two $\mathbf{q}$-modes of the form

$$\vec{\mathcal{S}}_x = S_0 \begin{pmatrix} 1 \\ 0 \\ 0 \end{pmatrix}, \quad \vec{\mathcal{S}}_y = S_0 \begin{pmatrix} 0 \\ 1 \\ 0 \end{pmatrix}, \tag{22}$$

with $S_0$ a real constant. In real space this corresponds to

$$\langle \vec{S}_j \rangle = S_0 \begin{pmatrix} \cos(\mathbf{Q}_x\cdot\mathbf{r}_j) \\ \cos(\mathbf{Q}_y\cdot\mathbf{r}_j) \\ 0 \end{pmatrix}. \tag{23}$$

This phase also has charge modulations in both directions, proportional to $[\cos(\mathbf{Q}_x\cdot\mathbf{r}_j)]^2 + [\cos(\mathbf{Q}_y\cdot\mathbf{r}_j)]^2$, as shown in panel (f) of Fig 1.

### 2.3.7 Beat states

Sometimes one finds states whose dominant $\mathbf{q}$-components take the form (up to a lattice rotation) $\mathbf{Q}_x = (\pi - 2\pi\eta,\, \pi)$ and $\mathbf{Q}'_x = (\pi - 2\pi\eta',\, \pi)$ with $\eta \neq \eta'$. As shown in panel (g) of Fig. 1, in

these states there are unidirectional charge modulations and the spin patterns usually show beat-like modulations, since the spin components are sums of cosines with different wave numbers and phases. Such states are finite size artifacts. They arise when the "optimal" incommensurability $\eta_{\text{opt}}$ lies in between $\eta$ and $\eta'$, which is however not allowed by the finite size of the system (cf. Eq. (13)). In the thermodynamic limit, where any real value of $\eta$ is permitted, these states converge to a pure stripe or spiral phase.

### 2.3.8 Other collinear orders

In some cases all the spins are ordered collinearly, but not in the shape of Néel order, stripe order or collinear bidirectional stripes. As noted already by Zaanen and Gunnarsson [18], these states will likely be replaced by stripe states in the thermodynamic limit. For example, the lattice sizes treated in our calculations are too small to resolve stripes with wave vectors $\mathbf{Q}$ close to $(\pi, \pi)$, so that the system prefers to order in a more complex manner. Such a state, sketched in panel (h) of Fig. 1, can be viewed as a kind of stripe order where the lines of constant density, instead of lying parallel to the $x$ (or $y$) direction, form a ring. In these cases, one finds several nonzero components of $\vec{\mathcal{S}}_{\mathbf{q}}$.

### 2.3.9 Strange orders

In some cases one cannot classify a state by any of the previously described orders. Such states do not exhibit a simple structure in momentum space and often show complex charge patterns. These states will be referred to as "strange order". In the vast majority of cases, their spin order is coplanar. An example is sketched in panel (i) of Fig. 1. The strange states are also expected to disappear in the thermodynamic limit [39].

## 2.4 Results from unrestricted real space calculations

As a typical result from an unrestricted Hartree-Fock calculation on a finite lattice, a $(n, T)$ phase diagram obtained for $t' = -0.15t$ and $U = 3t$ on a $20\times20$ lattice [39] is shown in Fig. 2. The various states classified according to the above scheme are indicated by distinct colors. The black transition lines have been obtained from calculations in the thermodynamic limit, which will be described in the next section.

The transition temperature $T^*$ obtained in the thermodynamic limit (solid line) is very close to the transition temperature found for the finite system. For densities at and close to half-filling, the system is Néel ordered. With few exceptions, Néel order is also obtained in the entire electron-doped region (for $n > 1$). Not only $T^*$, but also the boundary of the Néel ordered region inside the magnetic regime obtained from the calculation in the thermodynamic limit (dashed line) agrees very well with the real-space finite size calculation.

On the hole-doped side, the calculation in the thermodynamic limit (described in the next section) yields a regime of stable spiral order with a continuously varying incommensurability $\eta$ between the dashed and the dotted black lines in Fig. 2. In the real space calculation on the

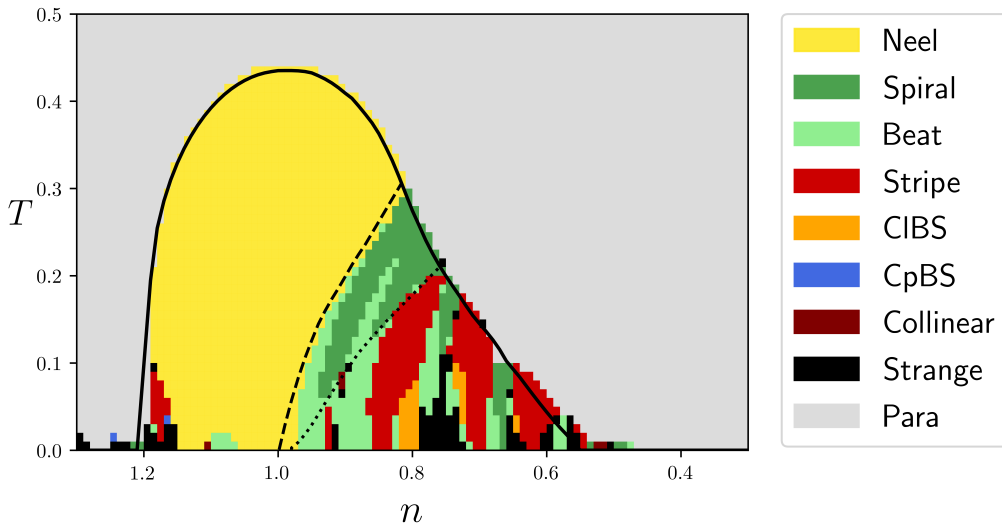


**Fig. 2:** *Phase diagram for $U = 3t$ and $t' = -0.15t$. The colors label the states resulting from the real space calculation on a $20\times20$ lattice. The black lines were obtained from calculations in momentum space in the thermodynamic limit. The solid black line indicates the transition temperature $T^*$ separating the paramagnetic from the magnetically ordered regime, the dashed black line the transition between Néel and spiral order, and the dotted black line the divergence of the charge susceptibility in the spiral state. Figure taken from Ref. [39].*

$20\times20$ lattice, the spiral regime is split into spiral and beat order regions, where the incommensurabilities in the spiral regions are either $\eta = 0.05$ (close to the Néel region) or $\eta = 0.1$. At densities and temperatures where one finds beat states it is energetically more costly for the system to order as a spiral state with the discrete incommensurabilities 0.05 or 0.1 allowed on the $20\times20$ lattice. Since intermediate ordering vectors are prohibited due to the periodic boundary conditions, the system orders in a beat ordered pattern. Looking at the wavevectors of the Fourier modes $\vec{\mathcal{S}}_{\mathbf{q}}$ in these states, one finds $\mathbf{Q}' = (\pi - 2\pi\frac{1}{20}, \pi)$ and $\mathbf{Q}'' = (\pi - 2\pi\frac{1}{10}, \pi)$. Solving the mean-field equations in the beat region between the spiral states on a $40\times40$ lattice one finds that beat order is indeed replaced by spiral order with an intermediate wavevector $\mathbf{Q} = (\pi - 2\pi\frac{3}{40}, \pi)$. Hence, the real space calculations are consistent with a spiral phase with a smoothly varying $\eta$.

Below the dotted line in Fig. 2, and for any temperature at densities below $n \approx 0.75$, spiral states exhibit negative (for some wave vectors) spin and charge susceptibilities, and are thus unstable. In this region stripes, other collinear states, and strange states appear. The stripe region is split into several domains with distinct incommensurabilities: $\eta = 0.05$ for densities $n \approx 0.93$, $\eta = 0.1$ for densities close to $n \approx 0.82$, $\eta = 0.15$ for densities around 0.7, and $\eta = 0.2$ near $n \approx 0.62$. These stripe regimes are separated by intermediate regions of beat ordered and strange phases, where the predominant wavevectors are the ones of the two adjacent stripe regimes. Repeating the calculation on a larger $40\times40$ lattice for a few $(n, T)$ pixels in this intermediate regime, one finds stripes with intermediate values of $\eta$. This confirms the hypothesis that beat and strange states are just artifacts of the finite system size.

A particular point in parameter space has received special attention in recent years: the ground state ($T$=0) at a density $n = \frac{7}{8}$ for the two-dimensional Hubbard model with pure nearest

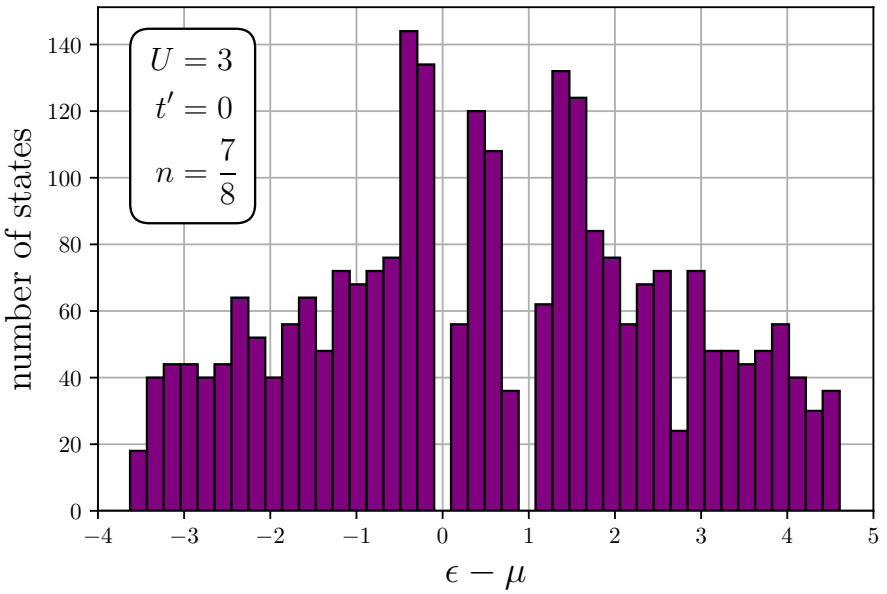


**Fig. 3:** *Density of states histogram for $n = \frac{7}{8}$, $T = 0$, $t' = 0$ and $U = 3t$, calculated on a $32\times40$ lattice. The states are counted in equidistant bins in the energy range between –4 and 5. Figure taken from Ref. [39].*

neighbor hopping. Exact numerical ground state techniques have provided fairly convincing evidence that for strong coupling the ground state is an insulating stripe state in this case [27–29]. Hence, it is interesting to investigate this special point in more detail, keeping however a moderate interaction strength $U = 3t$, in line with the Hartree-Fock approximation.

The solution of the real-space mean-field equations unambiguously yields unidirectional stripes with an incommensurability $\eta = \frac{1}{16}$ in this case. To see whether this stripe ground state is an insulator, one may look at the distribution of energy levels, which is a finite size proxy to the density of states. In Fig. 3, a histogram of the distribution of the energy levels $\varepsilon_\ell$ is shown, shifted by the chemical potential (placed half-way between the highest occupied and the lowest unoccupied state). One can see that there are no energy levels close to the chemical potential – there is a sizable band gap ($\Delta \approx 0.25t$). This stripe state is therefore indeed an insulator. There are other special choices of parameters leading to an insulating ground state, but metallic behavior is much more common.

# 3 Mean-field solutions in the thermodynamic limit

For several specific types of magnetic order, the Hartree-Fock equations can be solved directly in the thermodynamic limit. Among these, spiral states are particularly easy to treat, for any ordering wave vector $\mathbf{Q}$. The Néel state can be viewed as a special case of spiral order. More generally, any magnetic order can be treated in the thermodynamic limit if it is commensurate with the lattice, that is, if some (reduced) translation invariance remains in the ordered state. Finally, for temperatures slightly below the critical temperature $T^*$, an expansion in powers of the order parameter can help to discriminate distinct magnetic states.

## 3.1 Néel and spiral states

For circular spiral states, the mean-field equations assume a particularly simple form in momentum space, for arbitrary (also incommensurate) ordering wave vectors $\mathbf{Q}$ [4–13]. This is due to a residual translation symmetry of the ordered state, consisting of a lattice translation combined with a rotation in spin space. In the special case $\mathbf{Q} = (\pi, \pi)$, spiral order is just Néel order.
Choosing the spin order to lie in the $xy$ plane, the expectation value $\langle \vec{S}_j \rangle$ has the form Eq. (17). A Fourier transformation reveals that this type of order is associated with anomalous expectation values $\langle c^\dagger_{\mathbf{k}\uparrow} c_{\mathbf{k}+\mathbf{Q}\downarrow} \rangle$ in momentum space, and the mean-field interaction term (3) simplifies to

$$H^{\mathrm{MF}}_{\mathrm{int}} = -\sum_{\mathbf{k}} \left( \Delta^* c^\dagger_{\mathbf{k}\uparrow} c_{\mathbf{k}+\mathbf{Q}\downarrow} + \Delta c^\dagger_{\mathbf{k}+\mathbf{Q}\downarrow} c_{\mathbf{k}\uparrow} \right) + L|\Delta|^2/U \,, \tag{24}$$

with the self-consistency condition $\Delta = UL^{-1} \sum_{\mathbf{k}} \langle c^\dagger_{\mathbf{k}\uparrow} c_{\mathbf{k}+\mathbf{Q}\downarrow} \rangle$. Defining the two-component spinor $\Psi_{\mathbf{k}} = (c_{\mathbf{k}\uparrow}, c_{\mathbf{k}+\mathbf{Q}\downarrow})$, the mean-field Hamiltonian can be written in the concise form

$$H^{\mathrm{MF}} = \sum_{\mathbf{k}} \Psi^\dagger_{\mathbf{k}} \begin{pmatrix} \varepsilon_{\mathbf{k}} & -\Delta^* \\ -\Delta & \varepsilon_{\mathbf{k}+\mathbf{Q}} \end{pmatrix} \Psi_{\mathbf{k}} + L|\Delta|^2/U \,. \tag{25}$$

Its diagonalization yields two quasi-particle bands with dispersion relations

$$E^{\pm}_{\mathbf{k}} = \varepsilon^{+}_{\mathbf{k}} \pm \sqrt{(\varepsilon^{-}_{\mathbf{k}})^2 + |\Delta|^2} \,, \tag{26}$$

where $\varepsilon^{\pm}_{\mathbf{k}} = \frac{1}{2}(\varepsilon_{\mathbf{k}} \pm \varepsilon_{\mathbf{k}+\mathbf{Q}})$. The free energy is then obtained in the form

$$F = -T \sum_{\mathbf{k}} \sum_{\ell=\pm} \ln \left( 1 + e^{-\beta(E^\ell_{\mathbf{k}} - \mu)} \right) + L|\Delta|^2/U + \mu N \,. \tag{27}$$

The magnetic gap $\Delta$ and the ordering wave vector $\mathbf{Q}$ are obtained by minimizing $F$. Minimization with respect to $\Delta$ yields the gap equation

$$\Delta = \frac{U\Delta}{L} \sum_{\mathbf{k}} \frac{f(E^-_{\mathbf{k}} - \mu) - f(E^+_{\mathbf{k}} - \mu)}{2\sqrt{(\xi^-_{\mathbf{k}})^2 + |\Delta|^2}} \,, \tag{28}$$

where $f$ is the Fermi distribution. The free energy does not depend on the phase of $\Delta$, which can therefore be chosen arbitrarily. The optimal wave vector has usually the "axial" form $\mathbf{Q} = (Q, \pi)$, degenerate with $(\pi, Q)$, or sometimes the "diagonal" form $\mathbf{Q} = (Q, \pm Q)$.
To probe the stability of the spiral state obtained from solving the mean-field equations with a spiral ansatz, one can check whether the static (zero frequency) spin and charge susceptibilities in the spiral state are positive for all wave vectors $\mathbf{q}$. The combined spin and charge susceptibility is a $4\times4$ matrix with matrix elements $\chi^{ab}$, where the indices $a, b = 0, 1, 2, 3$ label charge $(0)$ and spin $(1, 2, 3)$ components [10, 43]. In a rotated spin frame, where the spiral state looks translation invariant, its Fourier transform $\widetilde{\chi}^{ab}(\mathbf{q}, \omega)$ depends only on a single wave vector. The conserving approximation [44] for susceptibilities corresponding to mean-field theory for the free energy is given by the so-called random phase approximation (RPA). In the rotated spin frame, the RPA susceptibility can be written as [10, 43],

$$\widetilde{\chi}(\mathbf{q}, \omega) = \widetilde{\chi}_0(\mathbf{q}, \omega) \big[ \mathbf{1}_4 - \Gamma_0 \widetilde{\chi}_0(\mathbf{q}, \omega) \big]^{-1} \,, \tag{29}$$

where $\Gamma_0 = 2U\,\mathrm{diag}(-1,1,1,1)$, and the bare susceptibility $\widetilde{\chi}_0(\mathbf{q},\omega)$, is given by

$$\widetilde{\chi}_0^{ab}(\mathbf{q},\omega) = -\frac{T}{4L}\sum_{\mathbf{k}}\sum_{k_0}\mathrm{Tr}\left[\sigma^a G(\mathbf{k}{+}\mathbf{q}, ik_0{+}iq_0)\,\sigma^b\,G(\mathbf{k},ik_0)\right]\Big|_{iq_0\to\omega+i0^+}, \tag{30}$$

where $G(\mathbf{k},ik_0)$ is the mean-field single-particle Green function in the spinor basis defined by $\Psi_{\mathbf{k}}$, the sum over $k_0$ is a sum over fermionic Matsubara frequencies, and $\sigma^0$ is the two-dimensional unit matrix, while $\sigma^1$, $\sigma^2$, $\sigma^3$ are the Pauli matrices.

## 3.2 Commensurate coplanar states

For *commensurate* order, the system retains some (reduced) translation invariance. Defining a suitable unit cell in the ordered state, the mean-field equations can then be solved in the thermodynamic limit. With very few exceptions, which are probably finite size artifacts, the spin order found in the unrestricted real space calculations is *coplanar*, that is, all the spins align in a common plane. Except for very large hole-doping in the presence of a large $|t'/t|$, the order is also *unidirectional*, that is, at most one (for Néel order none) of the two components of the contributing wave vectors is $\neq \pi$, such that spins order antiferromagnetically in one of the directions $x$ or $y$, and the electron density is homogeneous in this direction. In the present context it is therefore worthwhile to formulate and evaluate the mean-field equations for commensurate, coplanar, and unidirectional order in a momentum space representation [40]. Unidirectional collinear stripe and circular spiral order are special cases thereof.

Due to the SU(2) symmetry of the Hubbard model, the coplanar order can lie in any (fixed) plane in spin space. We select the $xy$ plane as a convenient choice, and we choose the $y$ direction in real space as the direction of simple antiferromagnetic order. In $x$ direction, we assume that the ordered state is periodic with a periodicity $P$. The magnetization and charge density profiles can then be expanded in Fourier modes as follows

$$\vec{S}_j = \sum_{n\ \mathrm{odd}}\left(M_n^x\vec{e}_x + M_n^y\vec{e}_y\right)e^{i\mathbf{Q}_n\cdot\mathbf{r}_j}, \tag{31a}$$

$$\rho_j = \sum_{n\ \mathrm{even}}\varrho_n\,e^{i\mathbf{Q}_n\cdot\mathbf{r}_j}, \tag{31b}$$

where $\mathbf{Q}_n = (2\pi n/P,\,\pi n)$ with $n = 0,\ldots,\bar{P}{-}1$, and $\vec{e}_x$ and $\vec{e}_y$ are unit vectors in the $x$ and $y$ direction, respectively. The first sum is running only over odd integers $n$ because the spin order is antiferromagnetic in $y$-direction, while the second sum is restricted to even integers since $\rho_j$ is translation invariant in $y$-direction. We define $\bar{P}$ as the smallest positive integer satisfying $\mathbf{Q}_{\bar{P}} = (0,0)$ modulo reciprocal lattice vectors. If $P$ is even, one has $\bar{P} = P$, and $\bar{P} = 2P$ if $P$ is odd. The summations in Eq. (31) run over a finite number $(\bar{P}/2)$ of terms. Since the spin and charge densities are real, the coefficients $M_n^x$, $M_n^y$, and $\varrho_n$ must obey

$$M_n^x = (M_{-n}^x)^* = (M_{\bar{P}-n}^x)^*, \tag{32a}$$

$$M_n^y = (M_{-n}^y)^* = (M_{\bar{P}-n}^y)^*, \tag{32b}$$

$$\varrho_n = (\varrho_{-n})^* = (\varrho_{\bar{P}-n})^*. \tag{32c}$$

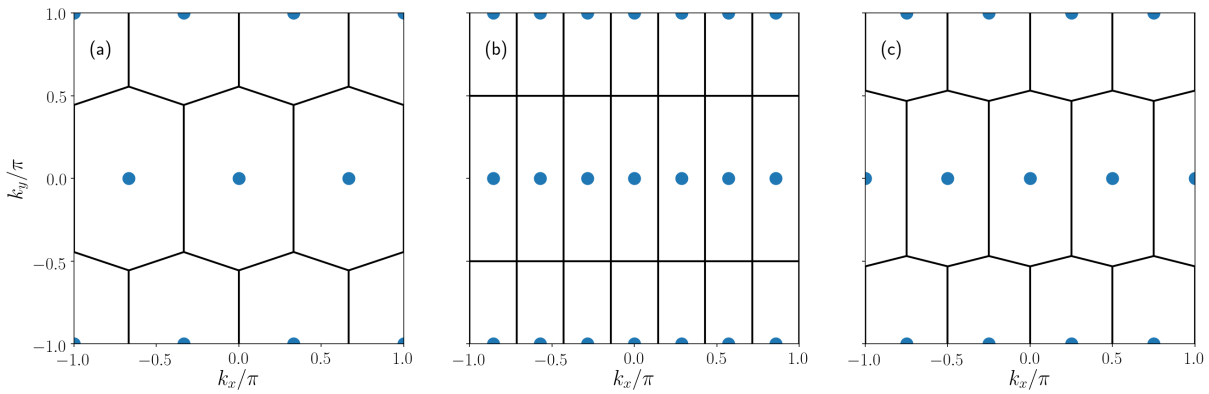


**Fig. 4:** *Construction of the reduced Brillouin zone for $P = 6$ (a), $P = 7$ (b), and $P = 8$ (c). The blue dots represent the momenta $\mathbf{Q}_n$ with $n = 0, ..., \bar{P}-1$ modulo vectors of the original reciprocal lattice. The black lines separate distinct reduced Brillouin zones. The original Brillouin zone is divided into $\bar{P}$ equivalent reduced Brillouin zones. Figure taken from [40].*

The translational symmetry breaking of the original lattice leads to an enlarged unit cell containing $\bar{P}$ inequivalent sites with distinct expectation values. In momentum space, the size of the original Brillouin zone is reduced by a factor $1/\bar{P}$. The new reciprocal lattice can be constructed by adding all vectors of the form $\mathbf{Q}_n$ with $n = 0, ..., \bar{P}-1$ to the original reciprocal lattice vectors (see Fig. 4). The reduced Brillouin zone can then be defined as the set of all points which are closer to a given vector of the new reciprocal lattice than to any other (Wigner-Seitz construction). The reduced Brillouin zones for $P = 6, 7, 8$ are plotted in Fig. 4.
The mean-field interaction term Eq. (3) can be written in the following manifestly SU(2) symmetric form [40]

$$H_{\text{int}}^{\text{MF}} = \sum_j \sum_{a=0}^{3} s_a \left[ \Delta_j^a \, c_j^\dagger \sigma^a c_j - (\Delta_j^a)^2/U \right] , \tag{33}$$

where $c_j$ is the two-component spinor composed of $c_{j\uparrow}$ and $c_{j\downarrow}$. The sign $s_a$ is plus one in the charge channel ($a = 0$) and minus one in the spin channel ($a = 1, 2, 3$). The gap parameters $\Delta_j^a$ are defined by charge and spin expectation values as $\Delta_j^a = \frac{1}{2} U \langle c_j^\dagger \sigma^a c_j \rangle$. They are related to the previously defined gap parameters via $\Delta_j^0 = \frac{1}{2}(\Delta_{j\uparrow} + \Delta_{j\downarrow})$, $\Delta_j^1 = \frac{1}{2}(\Delta_{j+} + \Delta_{j-})$, $\Delta_j^2 = \frac{1}{2i}(\Delta_{j+} - \Delta_{j-})$, and $\Delta_j^3 = \frac{1}{2}(\Delta_{j\uparrow} - \Delta_{j\downarrow})$. Inserting Eq. (31) into Eq. (33), adding the kinetic term, and Fourier transforming, we obtain

$$H_{\text{MF}} = \sum_{\mathbf{k}} \varepsilon_{\mathbf{k}} \, c_{\mathbf{k}}^\dagger c_{\mathbf{k}} + \sum_{\mathbf{k}} \sum_{a=0}^{2} \sum_{n=0}^{\bar{P}-1} s_a \Delta_n^a \, c_{\mathbf{k}}^\dagger \sigma^a c_{\mathbf{k}+\mathbf{Q}_n} - L \sum_{a=0}^{2} \sum_{n=0}^{\bar{P}-1} s_a \frac{|\Delta_n^a|^2}{U} , \tag{34}$$

with

$$\Delta_n^0 = \begin{cases} \frac{1}{2} U \varrho_n & \text{for } n \text{ even} \\ 0 & \text{for } n \text{ odd} \end{cases} , \quad \Delta_n^{1,2} = \begin{cases} 0 & \text{for } n \text{ even} \\ U M_n^{x,y} & \text{for } n \text{ odd} \end{cases} . \tag{35}$$

Defining the $\bar{P}$-component spinor

$$\Psi_{\mathbf{k},\sigma} = \left( c_{\mathbf{k},\sigma}, c_{\mathbf{k}+\mathbf{Q}_1,\bar{\sigma}}, c_{\mathbf{k}+\mathbf{Q}_2,\sigma}, \ldots, c_{\mathbf{k}+\mathbf{Q}_{\bar{P}-2},\sigma}, c_{\mathbf{k}+\mathbf{Q}_{\bar{P}-1},\bar{\sigma}} \right) \tag{36}$$

with the convention $\bar{\uparrow} = \downarrow$ and $\bar{\downarrow} = \uparrow$, one can cast the Hamiltonian (34) in the form

$$H_{\mathrm{MF}} = \sum_{\mathbf{k}\in \mathrm{BZ}'} \sum_{\sigma} \Psi^{\dagger}_{\mathbf{k},\sigma} \mathcal{H}^{(P)}_{\mathbf{k},\sigma} \Psi_{\mathbf{k},\sigma}, \tag{37}$$

where the constant term in Eq. (34) has been dropped, and the momentum sum is restricted to the reduced Brillouin zone $\mathrm{BZ}'$. The matrix $\mathcal{H}^{(P)}_{\mathbf{k},\sigma}$ is composed of the elements

$$\left[\mathcal{H}^{(P)}_{\mathbf{k},\sigma}\right]_{\ell\ell'} = \begin{cases} \varepsilon_{\mathbf{k}+\mathbf{Q}_\ell} & \text{if} \quad \ell = \ell' \\ \Delta^{p(\ell)}_{\sigma,n} & \text{if} \quad \ell' = (\ell+n) \bmod \bar{P},\ n \text{ odd} \\ \Delta^{0}_{n} & \text{if} \quad \ell' = (\ell+n) \bmod \bar{P},\ n \text{ even} \end{cases}, \tag{38}$$

where $p(\ell) = +$ if $\ell$ is even and $p(\ell) = -$ if $\ell$ is odd, and

$$\begin{aligned} \Delta^{\pm}_{\uparrow,n} &= -(\Delta^{1}_{n} \pm i\Delta^{2}_{n})\,, \\ \Delta^{\pm}_{\downarrow,n} &= -(\Delta^{1}_{n} \mp i\Delta^{2}_{n})\,. \end{aligned} \tag{39}$$

Since $\Delta^0_0$ only shifts the chemical potential $\mu$, one may redefine $\mu$ as $\mu - \Delta^0_0$ and set $\Delta^0_0 = 0$. For example, for $P = 3$ and $P = 6$, the matrix $\mathcal{H}^{(P)}_{\mathbf{k},\sigma}$ has the form

$$\mathcal{H}^{(6)\,\text{or}\,(3)}_{\mathbf{k},\sigma} = \begin{pmatrix} \varepsilon_{\mathbf{k},0} & \Delta^{+}_{\sigma,1} & \Delta^{0}_{2} & \Delta^{+}_{\sigma,3} & \Delta^{0}_{4} & \Delta^{+}_{\sigma,5} \\ \Delta^{-}_{\sigma,5} & \varepsilon_{\mathbf{k},1} & \Delta^{-}_{\sigma,1} & \Delta^{0}_{2} & \Delta^{-}_{\sigma,3} & \Delta^{0}_{4} \\ \Delta^{0}_{4} & \Delta^{+}_{\sigma,5} & \varepsilon_{\mathbf{k},2} & \Delta^{+}_{\sigma,1} & \Delta^{0}_{2} & \Delta^{+}_{\sigma,3} \\ \Delta^{-}_{\sigma,3} & \Delta^{0}_{4} & \Delta^{-}_{\sigma,5} & \varepsilon_{\mathbf{k},3} & \Delta^{-}_{\sigma,1} & \Delta^{0}_{2} \\ \Delta^{0}_{2} & \Delta^{+}_{\sigma,3} & \Delta^{0}_{4} & \Delta^{+}_{\sigma,5} & \varepsilon_{\mathbf{k},4} & \Delta^{+}_{\sigma,1} \\ \Delta^{-}_{\sigma,1} & \Delta^{0}_{2} & \Delta^{-}_{\sigma,3} & \Delta^{0}_{4} & \Delta^{-}_{\sigma,5} & \varepsilon_{\mathbf{k},5} \end{pmatrix}. \tag{40}$$

The parameters $\Delta^a_n$ are self-consistently determined as

$$\Delta^{a}_{n} = \frac{U}{2L} \sum_{\mathbf{k}} \left\langle c^{\dagger}_{\mathbf{k}} \sigma^{a} c_{\mathbf{k}+\mathbf{Q}_n} \right\rangle = \frac{U}{2L} \sum_{\mathbf{k}\in \mathrm{BZ}'} \sum_{\sigma} \left\langle \Psi^{\dagger}_{\mathbf{k},\sigma} \Gamma^{a}_{n,\sigma} \Psi_{\mathbf{k},\sigma} \right\rangle, \tag{41}$$

where the matrices $\Gamma^{a,n}_{\sigma}$ have been defined as

$$\left[\Gamma^{0}_{n,\sigma}\right]_{\ell\ell'} = \begin{cases} 1 \text{ if } \ell' = (\ell+n) \bmod \bar{P},\ n \text{ even} \\ 0 \text{ otherwise} \end{cases} \tag{42a}$$

$$\left[\Gamma^{1}_{n,\sigma}\right]_{\ell\ell'} = \begin{cases} 1 \text{ if } \ell' = (\ell+n) \bmod \bar{P},\ n \text{ odd} \\ 0 \text{ otherwise} \end{cases} \tag{42b}$$

$$\left[\Gamma^{2}_{n,\sigma}\right]_{\ell\ell'} = \begin{cases} i(-1)^{\sigma+p(\ell)} \text{ if } \ell' = (\ell+n) \bmod \bar{P},\ n \text{ odd} \\ 0 \text{ otherwise} \end{cases} \tag{42c}$$

with $(-1)^{\uparrow} = +1$ and $(-1)^{\downarrow} = -1$.

Since $\mathcal{H}^{(P)}_{\mathbf{k},\uparrow}$ and $\mathcal{H}^{(P)}_{\mathbf{k},\downarrow}$ are related to each other by an inversion of the sign of $\Delta^2_n$, the expectation values on the right hand side of Eq. (41) take the same value for each of the two spin projections. Hence, one can simplify Eq. (41) to

$$\Delta^a_n = UL^{-1} \sum_{\mathbf{k}\in \mathrm{BZ}'} \left\langle \Psi^\dagger_{\mathbf{k}} \Gamma^a_n \Psi_{\mathbf{k}} \right\rangle , \tag{43}$$

where $\Psi_{\mathbf{k}} = \Psi_{\mathbf{k},\uparrow}$ and $\Gamma^a_n = \Gamma^a_{n,\uparrow}$. In other words, one can solve the mean-field equations using only the matrix $\mathcal{H}^{(P)}_{\mathbf{k},\uparrow}$. The right hand side of Eq. (43) is computed from Eq. (38) making an initial random assumption on the mean-field parameters $\Delta^a_n$, which are then updated using again Eq. (43). The procedure is repeated until convergence is reached.

To find the energetically best state, one needs to solve Eq. (43) for different values of $P$ and retain the state with the lowest mean-field free-energy. In Ref. [40], the original Brillouin zone BZ was discretized with $N_k^2$ equally spaced points and, for a fixed $N_k$, only divisors of $N_k$ where admitted as possible values for $P$. For every fixed set of parameters, over 90 integer values of $P$ ranging from 2 to 220 were offered, each of them with a suitably adjusted $N_k$ such that $N_k/P$ is integer.

It is instructive to see how Néel, spiral, and collinear stripe states are captured as special cases of the above general formalism.

### 3.2.1 Néel order

In the case of Néel order, one has

$$\vec{S}_j = M(-1)^j \big( \cos\varphi\, \vec{e}_x + \sin\varphi\, \vec{e}_y \big) , \tag{44a}$$

$$\rho_j = \text{const.} , \tag{44b}$$

where $\varphi$ parametrizes the orientation of the spin order in the $xy$ plane, and $M$ represents its amplitude. Néel order has the period $P = 2$, so that the matrix $\mathcal{H}^{(P)}_{\mathbf{k},\sigma}$ in Eq. (38) is two-dimensional and only the two parameters $\Delta^1_1$ and $\Delta^2_1$ contribute, where

$$\Delta^1_1 = \Delta \cos\varphi , \quad \Delta^2_1 = \Delta \sin\varphi , \tag{45}$$

with $\Delta = UM$.

### 3.2.2 Circular spiral order

Circular spiral order in the $xy$ plane has the general form

$$\vec{S}_j = M\big( \cos(\mathbf{Q}\cdot\mathbf{r}_j + \varphi)\, \vec{e}_x \pm \sin(\mathbf{Q}\cdot\mathbf{r}_j + \varphi)\, \vec{e}_y \big) , \tag{46a}$$

$$\rho_j = \text{const.} , \tag{46b}$$

where, as in the case of Néel order, $\varphi$ parametrizes the orientation of the spin order in the $xy$ plane and $M$ its (constant) amplitude. $\mathbf{Q}$ is a generic wave vector of the form $(\pi - 2\pi\eta,\, \pi)$ with $\eta > 0$. The "+" or "–" sign distinguishes between spirals rotating anti-clockwise and clockwise.

This type of order emerges as a special case of our general formalism if $\Delta_n^a$ is non-zero only for one mode $n_0$ and its conjugate $\bar{P}-n_0$, with $n_0$ odd and such that $\mathbf{Q}$ can be approximated by $\mathbf{Q}_{n_0}$, with a suitably chosen $P$. Spiral order as in Eq. (46) is then described by

$$\Delta_{n_0}^1 = \tfrac{1}{2}\Delta e^{i\varphi}\,, \qquad \Delta_{\bar{P}-n_0}^1 = \frac{1}{2}\Delta e^{-i\varphi}\,, \tag{47a}$$

$$\Delta_{n_0}^2 = \mp\tfrac{i}{2}\Delta e^{i\varphi}\,, \qquad \Delta_{\bar{P}-n_0}^2 = \pm\frac{i}{2}\Delta e^{-i\varphi}\,, \tag{47b}$$

with $\Delta = UM$. All other $\Delta_n^a$ are zero. The matrix $\mathcal{H}_{\mathbf{k},\sigma}^{(P)}$ thus simplifies to a diagonal block matrix form with $\bar{P}/2$ matrices of size two on the diagonal. Indeed spiral order can be described by a simpler $2\times2$ mean-field Hamiltonian for each $\mathbf{k}$-point, as described above. Eqs. (47) apply only if $n_0 \neq \bar{P}-n_0$, which is fulfilled for any spiral state which is not a Néel state.

### 3.2.3 Stripe order

Defining stripe order as any type of collinear order that differs from Néel antiferromagnetism, the magnetization and charge densities have the form

$$\vec{S}_j = f_S(\mathbf{r}_j)\big(\cos\varphi\,\vec{e}_x + \sin\varphi\,\vec{e}_y\big)\,, \tag{48a}$$

$$\rho_j = f_\rho(\mathbf{r}_j)\,, \tag{48b}$$

where once again $\varphi$ is an angle parameterizing the orientation of the spins in the $xy$ plane, while $f_S(\mathbf{r}_j)$ and $f_\rho(\mathbf{r}_j)$ are two functions defining the spatial modulation of the magnetization amplitude and charge density, respectively. They can be expressed in terms of their Fourier coefficients as

$$f_S(\mathbf{r}_j) = \sum_{n\,\mathrm{odd}} M_n\, e^{i\mathbf{Q}_n\cdot\mathbf{r}_j}\,, \tag{49a}$$

$$f_\rho(\mathbf{r}_j) = \sum_{n\,\mathrm{even}} \rho_n\, e^{i\mathbf{Q}_n\cdot\mathbf{r}_j}\,. \tag{49b}$$

Stripe order can be obtained as a particular case of the general formalism, with $\Delta_n^a$ fulfilling

$$\Delta_n^0 = U\rho_n\,, \quad \Delta_n^1 = UM_n\cos\varphi\,, \quad \Delta_n^2 = UM_n\sin\varphi\,. \tag{50}$$

Depending on the coefficients $M_n$ and $\rho_n$, the spin and charge profiles can be sinusoidal or sharp (like domain walls) or anything in between.

## 3.3 Landau theory

Slightly below the critical temperature $T^*$, the type of magnetic order can be determined from the Landau theory of the phase transition, which is valid for small order parameters. The Landau theory can be derived from the microscopic (mean-field) theory by decoupling the Hubbard interaction with spin and charge order parameter fields via a Hubbard-Stratonovich transformation, and subsequently expanding the resulting effective action in powers of the order parameters. In this section we need to use the path-integral formalism for quantum many-body systems, as described, for example, in the textbook by Negele and Orland [45].

### 3.3.1 Derivation of the effective action

The Hubbard interaction can be written in the SU(2) symmetric form [46–48]

$$U n_{j\uparrow} n_{j\downarrow} = \frac{U}{4}\big(c_j^\dagger c_j\big)^2 - \frac{U}{4}\big(c_j^\dagger\, \vec{\sigma}\cdot\vec{n}_j\, c_j\big)^2\,, \tag{51}$$

where $\vec{n}_j$ is an arbitrary unit vector. In the path integral formalism, the operators $c_j$ and $c_j^\dagger$ are replaced by time dependent anticommuting (Grassmann) fields $c_j(\tau)$ and $c_j^*(\tau)$, respectively. Because $\vec{n}_j$ can be arbitrarily chosen, we take the average over all possible $\vec{n}_j$ with a properly defined measure such that $\int \mathcal{D}\vec{n} = 1$.
Performing a Hubbard-Stratonovich transformation [45], the interaction terms in Eq. (51) can be decoupled by means of two fields, $\rho_j(\tau)$ and $\rho_j^S(\tau)$, representing space and (imaginary) time dependent fluctuations of the charge and spin amplitude, respectively. Defining a spin field as $\vec{S}_j(\tau) = \rho_j^S(\tau)\,\vec{n}_j(\tau)$, the Hubbard interaction can be represented as

$$e^{-U\int_0^\beta d\tau \sum_j n_{j\uparrow}n_{j\downarrow}} = \int \mathcal{D}\rho\,\mathcal{D}\vec{S}\, e^{-(\mathcal{S}_\rho+\mathcal{S}_S+\mathcal{S}_{\text{int}})}\,, \tag{52}$$

where $\beta = 1/T$ is the inverse temperature, and

$$\mathcal{S}_\rho = \frac{1}{U}\int_0^\beta d\tau \sum_j \rho_j^2\,, \tag{53a}$$

$$\mathcal{S}_S = \frac{1}{U}\int_0^\beta d\tau \sum_j |\vec{S}_j|^2\,, \tag{53b}$$

$$\mathcal{S}_{\text{int}} = \int_0^\beta d\tau \sum_j c_j^*(i\rho_j + \vec{S}_j\cdot\vec{\sigma})c_j\,. \tag{53c}$$

To keep the notation light, the time dependence of the bosonic ($\rho_j$, $\vec{S}_j$) and fermionic ($c_j$, $c_j^*$) fields is not written.
An effective action for the bosonic fields $\rho_j$ and $\vec{S}_j$ can be derived by integrating out the fermions. Except for a field-independent term, one obtains

$$\mathcal{S}^{\text{eff}}\big[\rho,\vec{S}\big] = \frac{1}{U}\int_0^\beta d\tau \sum_j \big(\rho_j^2 + |\vec{S}_j|^2\big) - \operatorname{tr}\ln\Big[1_{\text{st}} - G_0\cdot\big(i\rho + \vec{\sigma}\cdot\vec{S}\big)\Big]\,, \tag{54}$$

where $G_0$ is the Fourier transform to real space and imaginary time of the bare Matsubara Green function $G_0(k) = (i\nu+\mu-\varepsilon_{\mathbf{k}})^{-1}$, while $\rho$ and $\vec{S}$ are diagonal matrices in space and time defined as $\rho_{jj'}(\tau,\tau') = \rho_j(\tau)\,\delta_{jj'}\delta(\tau-\tau')$ and $\vec{S}_{jj'}(\tau,\tau') = \vec{S}_j(\tau)\,\delta_{jj'}\delta(\tau-\tau')$. The trace is summing over space and time indices, $1_{\text{st}} = \delta_{jj'}\delta(\tau-\tau')$ is the space-time unit matrix, and $G_0A$ is the space-time matrix product $\sum_{j''}\int_0^\beta d\tau''\, G_{0,jj''}(\tau-\tau'')\,A_{j''j'}(\tau'',\tau')$.

### 3.3.2 Taylor expansion of the effective action

We now expand the logarithm in Eq. (54) in powers of $\rho_j$ and $\vec{S}_j$. Such an expansion is justified in the vicinity of the critical temperature $T^*$, where the magnetic and charge order parameters

are small. To this end we write

$$\mathrm{tr}\ln\left[1_{\mathrm{st}} - G_0 A\right] = -\sum_{n=1}^{\infty} \frac{1}{n}\,\mathrm{tr}\left[(G_0 A)^n\right]\,, \tag{55}$$

with $A = i\rho + \vec{\sigma}\cdot\vec{S}$. The trace does not depend on the representation. In the following, all calculations are performed in momentum and frequency space.
The quadratic term in $\vec{S}_q$, the (spatio-temporal) Fourier transform of $\vec{S}_j(\tau)$, takes the form

$$\int_q \left[U^{-1} - \Pi_0(q)\right] \vec{S}_{-q}\cdot\vec{S}_q\,, \tag{56a}$$

$$\Pi_0(q) = -\int_k G_0(k)\, G_0(k{+}q)\,. \tag{56b}$$

Here and in the following, $k = (\mathbf{k}, ik_0)$ and $q = (\mathbf{q}, iq_0)$ are collective variables comprising lattice momenta and Matsubara frequencies, and $\int_k = T\sum_{k_0}\int \frac{d^2\mathbf{k}}{(2\pi)^2}$ is a shorthand notation for a Matsubara frequency sum and a momentum integration. We define $T^*$ as the critical temperature where $\min_{\mathbf{q}}\left[U^{-1}{-}\Pi_0(\mathbf{q},0)\right] = 0$, signaling an instability towards the formation of magnetic order. This condition is first met, in the most general case, at four symmetry related wave vectors in the Brillouin zone of the form $\mathbf{q} = \pm\mathbf{Q}_x$ or $\mathbf{q} = \pm\mathbf{Q}_y$, with $\mathbf{Q}_x = (\pi{-}2\pi\eta,\,\pi)$ and $\mathbf{Q}_y = (\pi,\,\pi{-}2\pi\eta)$. This means that the magnetic order forming right below $T^*$ can be characterized by these wave vectors. Note that, because of the opposite sign between the two terms on the right hand side of Eq. (51), the coefficient of the term quadratic in $\rho_q$ is $U^{-1} + \Pi_0(q)$, which is always positive. Thus, within mean-field theory, an instability towards charge order alone can never occur in the Hubbard model.
For a mean-field study of the Taylor-expanded effective action (54), we can thus assume that $\vec{S}_q$ possesses solely modes at $\mathbf{q}{=}\pm\mathbf{Q}_x$ and $\mathbf{q}{=}\pm\mathbf{Q}_y$ close to $T{=}T^*$, corresponding to the ansatz

$$\vec{S}_q = \Big[\vec{M}_x\,\delta(\mathbf{q}{-}\mathbf{Q}_x) + \vec{M}_x^*\,\delta(\mathbf{q}{+}\mathbf{Q}_x) + \vec{M}_y\,\delta(\mathbf{q}{-}\mathbf{Q}_y) + \vec{M}_y^*\,\delta(\mathbf{q}{+}\mathbf{Q}_y)\Big]\delta_{q_0,0}\,, \tag{57}$$

where $\vec{M}_x$ and $\vec{M}_y$ are constant complex vectors. We assume static fields, consistent with our mean-field treatment.
Third order terms involving only spin fields vanish due to time-reversal symmetry. The third order term involving two $\vec{S}_q$ fields and one $\rho_q$ field takes the form

$$\int_{q,q'} i\lambda(q,q')\vec{S}_q\cdot\vec{S}_{-q'}\rho_{q'-q}\,, \tag{58}$$

with a coupling function $\lambda(q,q')$. Inserting Eq. (57) into this equation, we see that, within mean-field theory, the only charge modes that couple to $\vec{M}_x$ and $\vec{M}_y$ are those where $\mathbf{q} = \mathbf{0}$, $\mathbf{q} = \pm 2\mathbf{Q}_x$, $\mathbf{q} = \pm 2\mathbf{Q}_y$ and $\mathbf{q} = \pm(\mathbf{Q}_x{\pm}\mathbf{Q}_y)$. Neglecting the $\mathbf{q} = \mathbf{0}$ mode, which does not lead to any symmetry breaking, and higher order spin-charge interactions (this approximation will be justified below), we can write

$$\begin{aligned} i\rho_q = \big[\;&\phi_x\,\delta(\mathbf{q}{-}2\mathbf{Q}_x) + \phi_x^*\,\delta(\mathbf{q}{+}2\mathbf{Q}_x) + \phi_y\,\delta(\mathbf{q}{-}2\mathbf{Q}_y) + \phi_y^*\,\delta(\mathbf{q}{+}2\mathbf{Q}_y) \\ &+\phi_+\,\delta(\mathbf{q}{-}\,\mathbf{Q}_+) + \phi_+^*\,\delta(\mathbf{q}{+}\,\mathbf{Q}_+) + \phi_-\,\delta(\mathbf{q}{-}\,\mathbf{Q}_-) + \phi_-^*\,\delta(\mathbf{q}{+}\,\mathbf{Q}_-)\big]\delta_{q_0,0}\,, \end{aligned} \tag{59}$$

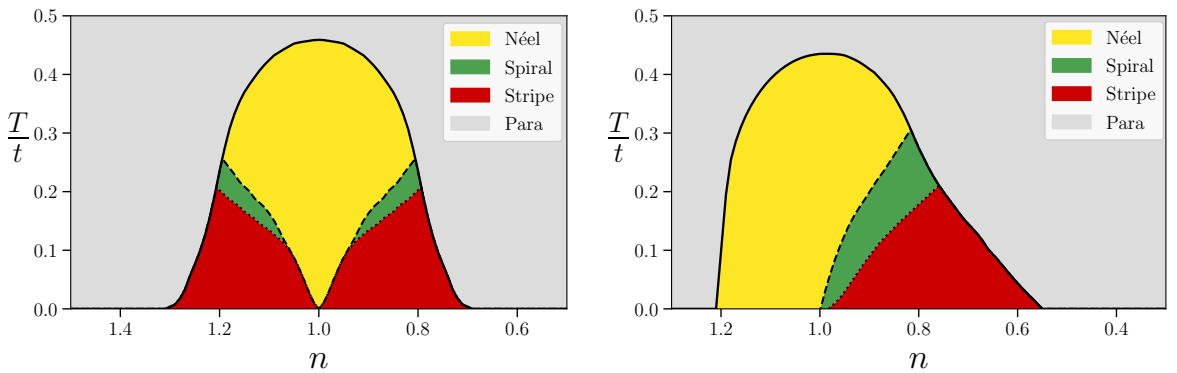


**Fig. 5:** *Mean field phase diagrams in the thermodynamic limit for $U = 3t$ with $t' = 0$ (left) and $t' = -0.15t$ (right). All transition lines have been computed in the thermodynamic limit. The magnetic order in the "stripe" regime is always coplanar, but not necessarily collinear. Figures taken from Ref. [39].*

where $\phi_x$, $\phi_y$, and $\phi_\pm$ are complex constants, and $\mathbf{Q}_\pm = \mathbf{Q}_x \pm \mathbf{Q}_y$.
Inserting Eq. (57) and (59) into Eq. (54), and expanding up to quartic order in $\vec{M}_x$ and $\vec{M}_y$, to quadratic order in $\phi_x$, $\phi_y$, and $\phi_\pm$, and to third order in the mixed terms, we obtain the effective potential

$$\begin{aligned} V(\vec{M}_x, \vec{M}_y, \phi_x, \phi_y, \phi_\pm) &= s\left(|\vec{M}_x|^2 + |\vec{M}_y|^2\right) \\ &+ u_0\left(|\vec{M}_x|^2 + |\vec{M}_y|^2\right)^2 + u_1\left(|\vec{M}_x|^2 - |\vec{M}_y|^2\right)^2 \\ &+ u_2\left(|\vec{M}_x\cdot\vec{M}_x|^2 + |\vec{M}_y\cdot\vec{M}_y|^2\right) + u_3\left(|\vec{M}_x\cdot\vec{M}_y|^2 + |\vec{M}_x\cdot\vec{M}_y^*|^2\right) \\ &- r_1\left(|\phi_x|^2 + |\phi_y|^2\right) - r_2\left(|\phi_+|^2 + |\phi_-|^2\right) \\ &+ b_1\left(\phi_x\,\vec{M}_x^*\cdot\vec{M}_x^* + \phi_y\,\vec{M}_y^*\cdot\vec{M}_y^* + \text{c.c.}\right) \\ &+ b_2\left(\phi_+\,\vec{M}_x^*\cdot\vec{M}_y^* + \phi_-\,\vec{M}_x^*\cdot\vec{M}_y + \text{c.c.}\right) . \end{aligned} \tag{60}$$

The coefficients $s$, $u_0$, $u_1$, $u_2$, $u_3$, $r_1$, $r_2$, $b_1$, and $b_2$ are determined by frequency and momentum integrals of products of bare propagators $G_0$. The concrete expressions are presented in the Appendix.
The charge degrees of freedom can be eliminated from the theory by imposing $\partial V/\partial\phi_\alpha = 0$, for $\alpha = x, y, \pm$, which yields

$$\phi_x = \frac{b_1}{r_1}\vec{M}_x\cdot\vec{M}_x\,, \qquad \phi_y = \frac{b_1}{r_1}\vec{M}_y\cdot\vec{M}_y\,, \tag{61a}$$

$$\phi_+ = \frac{b_2}{r_2}\vec{M}_x\cdot\vec{M}_y\,, \qquad \phi_- = \frac{b_2}{r_2}\vec{M}_x\cdot\vec{M}_y^*\,. \tag{61b}$$

From the above equations we see that at the extremal points of the potential $V$ the charge order parameter is a bilinear of the spin order parameter. Therefore, in order to get an effective theory that is at most quartic in $\vec{M}_x$ and $\vec{M}_y$, one has to retain all and only the terms in Eq. (60) in the

expansion of the bosonic action (54). Inserting Eqs. (61) into (60), one gets

$$\begin{aligned} V_{\text{eff}}(\vec{M}_x, \vec{M}_y) = & \, s \left( |\vec{M}_x|^2 + |\vec{M}_y|^2 \right) \\ & + u_0 \left( |\vec{M}_x|^2 + |\vec{M}_y|^2 \right)^2 + u_1 \left( |\vec{M}_x|^2 - |\vec{M}_y|^2 \right)^2 \\ & + \tilde{u}_2 \left( |\vec{M}_x \cdot \vec{M}_x|^2 + |\vec{M}_y \cdot \vec{M}_y|^2 \right) + \tilde{u}_3 \left( |\vec{M}_x \cdot \vec{M}_y|^2 + |\vec{M}_x \cdot \vec{M}_y^*|^2 \right) \, , \end{aligned} \tag{62}$$

with $\tilde{u}_2 = u_2 + b_1^2/r_1$ and $\tilde{u}_3 = u_3 + b_2^2/r_2$. Minimizing $V_{\text{eff}}(\vec{M}_x, \vec{M}_y)$ with respect to $\vec{M}_x$ and $\vec{M}_y$ one can determine the magnetic state at temperatures right below $T^*$. A Landau theory with an effective potential of the form (62) has previously been derived from general symmetry arguments [41, 49, 50]. The form of the Landau theory restricted to the case of a single mode ($\vec{M}_x$ or $\vec{M}_y$) was derived earlier in Ref. [42].

## 3.4 Spiral to stripe transition and comprehensive phase diagrams

All calculations show that essentially three types of magnetic order can occur in the two-dimensional Hubbard model: Néel, spiral, and (in a broad sense) stripe. The stripe order is associated with charge order. Its spin order is usually collinear, but not always. The phase boundaries of these orders can be computed directly in the thermodynamic limit, as described above. In Fig. 5 the corresponding phase diagrams are shown for $U = 3t$ and two choices of $t'$. The phase diagram for $t' = 0$ is particle-hole symmetric. The ground state is Néel ordered only at half-filling in this case, and stripe ordered otherwise, while spiral order occurs only in a small region at finite temperatures. For $t' = -0.15t$, the entire electron doped regime is Néel ordered, and for small hole-doping there is now a spiral regime even in the ground state. As a general trend, the spiral regime becomes larger for a larger $|t'|$.

The Landau theory is consistent with the phase diagrams in Fig. 5. Minimizing the potential $V_{\text{eff}}(\vec{M}_x, \vec{M}_y)$ in Eq. (62), one obtains the same sequence of Néel, spiral, and stripe states close to $T^*$. For $t' = -0.3t$, the Landau theory yields a coplanar bidirectional stripe phase for very large hole doping ($n < 0.6$) [40].

For $T < T^*$, the regime labeled as "stripe" in Fig. 5 hosts actually two distinct types of order: a non-collinear phase near the spiral regime, and a collinear stripe phase at larger hole doping [40]. Both are stripe phases in the sense that they are associated with unidirectional charge order. The structure of the non-collinear phase is rather complex. It is a superposition of several spiral modulations with three or four distinct wave vectors. Two of them are determined by the wave vector at which the spin-charge susceptibility diverges upon approaching the boundary of the (single $\mathbf{Q}$) spiral regime. The "multi-spiral" regime between the conventional spiral and the collinear stripe phase is quite narrow, and its width shrinks to zero upon approaching $T^*$. A complete phase diagram showing all the phase transitions is provided in Fig. 6. The transition points at $T = 0$ and $T^*$ have been computed for $U = 3t$ and $t' = -0.3t$. The coplanar bidirectional stripe phase at very large hole doping (small $n$) does not exist for the smaller values of $|t'|$ in Fig. 5. The nature of the phase between the collinear unidirectional stripe phase and the coplanar bidirectional stripe phase (marked by a question mark) has not yet been clarified.

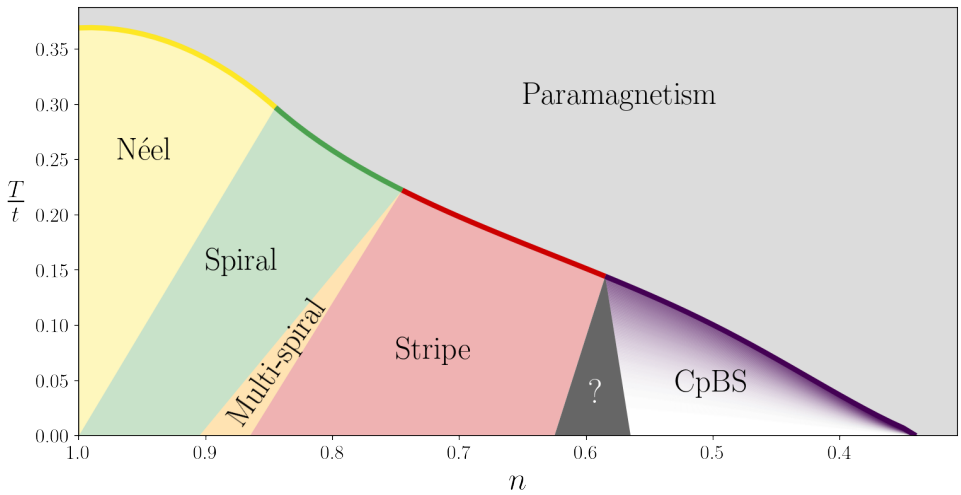


**Fig. 6:** *Mean field phase diagram for $U = 3t$ and $t' = -0.3t$. The various types of magnetic instabilities at $T^*$ were determined from the Landau theory, the states at $T = 0$ by solving the Hartree-Fock equations in the thermodynamic limit. The phase transitions for $0 < T < T^*$ are indicated only schematically by straight lines connecting the calculated transition points at $T = 0$ and $T = T^*$. Figure taken from Ref. [40].*

# 4 Renormalized mean-field theory

The Hartree-Fock theory discussed in the preceding sections yields valuable hints on possible magnetic ordering tendencies. However, it grossly overestimates the size of the ordered regimes, even in the ground state, and even for weak interaction strengths. Moreover, it completely misses the pairing instability, since the attractive $d$-wave pairing in the two-dimensional Hubbard model is purely fluctuation driven.

At weak or moderate interactions, these limitations can be overcome by a *renormalized* mean-field theory, where the mean-field equations are evaluated with renormalized (effective) interactions, which can be computed from a functional renormalization group (fRG) flow [51]. This fusion of the fRG with mean-field theory can be formulated quite systematically, and without any bias on a specific ordering channel [52].

A detailed discussion of the fRG+MF method is beyond the scope of these lectures. However, it is instructive to compare the resulting phase diagrams to those obtained from the plain Hartree-Fock approximation. A phase diagram obtained recently [53] from the renormalized mean-field theory with an unrestricted evaluation of the corresponding mean-field equations is shown in Fig. 7. The size of the magnetic regime is much smaller compared to the Hartree-Fock result, in spite of the larger interaction $U = 4t$. Indeed, the *effective* magnetic interaction is reduced by fluctuations to $U^m \approx 2t$. Moreover, a sizable effective $d$-wave pairing interaction $U^p$ leads to extended superconducting regimes, often coexisting with the magnetic order. Looking at details one can see that the presence of superconductivity favors spiral order over stripe order, and it suppresses magnetic order completely at the van Hove filling $n \approx 0.83$, where the Fermi level is situated at the van Hove singularity of the bare density of states.

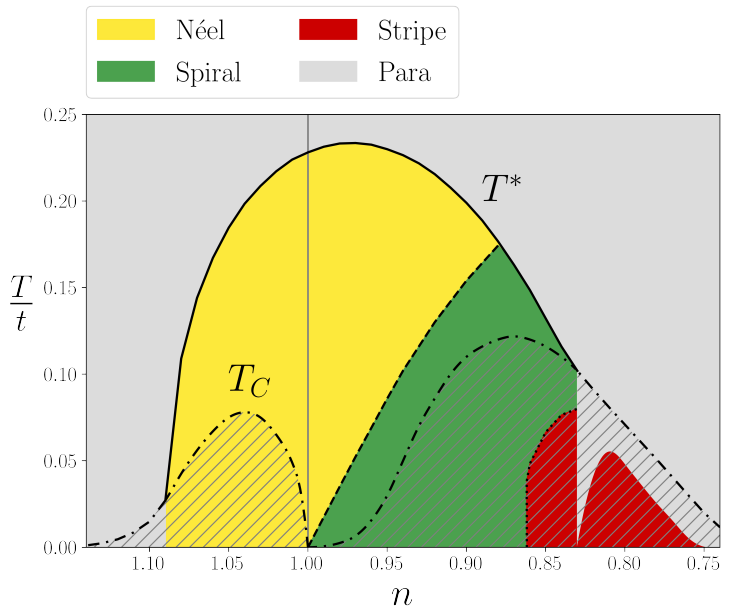


**Fig. 7:** $(n, T)$ *phase diagram of the two-dimensional Hubbard model for* $U = 4t$ *and* $t' = -0.2t$ *as obtained from renormalized mean-field theory. All the black lines have been computed directly in the thermodynamic limit. The solid line indicates the onset of magnetic order. The dash-dotted lines show the onset of superconductivity, and the shaded areas the superconducting regions. The dotted line indicates the instability of the spiral states, as signaled by a diverging charge susceptibility. Near the spiral region, the region labeled as "stripe" may also contain a non-collinear charge ordered state. The boundary of the small stripe-ordered dome at low densities could only be estimated from finite size calculations. Figure taken from Ref. [53].*

The Mermin-Wagner theorem prohibiting the spontaneous breaking of continuous symmetries at finite temperatures in two dimensions is violated also by the renormalized mean-field theory (as in plain Hartree-Fock). Hence, $T^*$ in Fig. 7 indicates only the onset of strong magnetic correlations, and $T_c$ the temperature scale for the formation of Cooper pairs. A complete theory needs to take order parameter fluctuations into account, but the renormalized mean-field theory is a useful starting point, and it identifies the key players in the intriguing interplay of competing correlations in the two-dimensional Hubbard model.

**Acknowledgement:** The material reviewed in these lecture notes is based on a wonderful collaboration with Robin Scholle, Pietro Bonetti, and Demetrio Vilardi [39, 40, 53].

# Appendix

## A Landau coefficients

In this section, the microscopic expressions for the coefficients of the effective potential in Eq. (60) are presented. The coefficients of the quadratic terms are given by

$$s = \frac{2}{U} - 2\Pi_0(Q_x) = \frac{2}{U} - 2\Pi_0(Q_y)\,, \tag{63a}$$

$$r_1 = \frac{2}{U} + 2\Pi_0(2Q_x) = \frac{2}{U} + 2\Pi_0(2Q_y)\,, \tag{63b}$$

$$r_2 = \frac{2}{U} + 2\Pi_0(Q_x{+}Q_y) = \frac{2}{U} + 2\Pi_0(Q_x{-}Q_y)\,, \tag{63c}$$

where the bare bubble $\Pi_0(q)$ has been defined in Eq. (56), and $Q_\alpha = (\mathbf{Q}_\alpha, 0)$ for $\alpha = x, y$. The third order coefficients $b_1$ and $b_2$ are given by

$$b_1 = 2\int_k G_0(k)\, G_0(k{+}Q_x)\, G_0(k{+}2Q_x) = \{x \leftrightarrow y\}\,, \tag{64a}$$

$$b_2 = 4\int_k G_0(k)\, G_0(k{+}Q_x)\, G_0(k{+}Q_x{+}Q_y) = \{x \leftrightarrow y\}\,. \tag{64b}$$

The fourth-order coefficients can be conveniently expressed in terms of the integrals

$$\begin{aligned}
E_1 &= \int_k G_0(k)\, G_0(k{+}Q_x)\, G_0(k{+}2Q_x)\, G_0(k{+}Q_x)\,,\\
E_2 &= \int_k G_0(k)\, G_0(k{+}Q_x)\, G_0(k)\, G_0(k{+}Q_x)\,,\\
E_3 &= \int_k G_0(k)\, G_0(k{+}Q_x)\, G_0(k)\, G_0(k{+}Q_y)\,,\\
E_4 &= \int_k G_0(k)\, G_0(k{+}Q_x)\, G_0(k{+}Q_x{+}Q_y)\, G_0(k{+}Q_y)\,,
\end{aligned} \tag{65}$$

in the form $u_0 = E_2{+}2E_3{-}E_4$, $u_1 = E_2{-}2E_3{+}E_4$, $u_2 = 2E_1{-}E_2$, and $u_3 = 4E_4$.

# References


[1] D.J. Scalapino, Rev. Mod. Phys. **84**, 1383 (2012)

[2] D.P. Arovas, E. Berg, S.A. Kivelson, and S. Raghu, Annu. Rev. Condens. Matter Phys. **13** 239 (2022)

[3] M. Qin, T. Schäfer, S. Andergassen, P. Corboz, and E. Gull, Annu. Rev. Condens. Matter Phys. **13** 275 (2022)

[4] B.I. Shraiman and E.D. Siggia, Phys. Rev. Lett. **62**, 1564 (1989)

[5] B.I. Shraiman and E.D. Siggia, Phys. Rev. B **46**, 8305 (1992)

[6] A.V. Chubukov and D.M. Frenkel, Phys. Rev. B **46**, 11884 (1992)

[7] A.V. Chubukov and K.A. Musaelian, Phys. Rev. B **51**, 12605 (1995)

[8] T. Dombre, J. Phys. France **51**, 847 (1990)

[9] R. Frésard, M. Dzierzawa, and P. Wölfle, Europhys. Lett. **15**, 325 (1991)

[10] A.P. Kampf, Phys. Rev. B **53**, 747 (1996)

[11] V.N. Kotov and O.P. Sushkov, Phys. Rev. B **70**, 195105 (2004)

[12] P.A. Igoshev, M.A. Timirgazin, A.A. Katanin, A.K. Arzhnikov, and V.Y. Irkhin, Phys. Rev. B **81**, 094407 (2010)

[13] H. Yamase, A. Eberlein, and W. Metzner, Phys. Rev. Lett. **116**, 096402 (2016)

[14] A. Eberlein, W. Metzner, S. Sachdev, and H. Yamase, Phys. Rev. Lett. **117**, 187001 (2016)

[15] J. Mitscherling and W. Metzner, Phys. Rev. B **98**, 195126 (2018)

[16] P.M. Bonetti, J. Mitscherling, D. Vilardi, and W. Metzner, Phys. Rev. B **101**, 165142 (2020)

[17] H.J. Schulz, J. Phys. France **50**, 2833 (1989)

[18] J. Zaanen and O. Gunnarsson, Phys. Rev. B **40**, 7391 (1989)

[19] D. Poilblanc and T.M. Rice, Phys. Rev. B **39**, 9749 (1989)

[20] H.J. Schulz, Phys. Rev. Lett. **64**, 1445 (1990)

[21] M. Kato, K. Machida, H. Nakanishi, and M. Fujita, J. Phys. Soc. Jpn. **59**, 1047 (1990)

[22] G. Seibold, C. Castellani, C. Di Castro, and M. Grilli, Phys. Rev. B **58**, 13506 (1998)

[23] M. Fleck, A.I. Lichtenstein, E. Pavarini, and A.M. Oleś, Phys. Rev. Lett. **84**, 4962 (2000)

[24] M. Raczkowski and F.F. Assaad, Phys. Rev. B **82**, 233101 (2010)

[25] R. Peters and N. Kawakami, Phys. Rev. B **89**, 155134 (2014)

[26] S.A. Kivelson, I.P. Bindloss, E. Fradkin, V. Oganesyan, J.M. Tranquada, A. Kapitulnik, and C. Howald, Rev. Mod. Phys. **75**, 1201 (2003)

[27] B.-X. Zheng, C.-M. Chung, P. Corboz, G. Ehlers, M.-P. Qin, R.M. Noack, H. Shi, S.R. White, S. Zhang, and G.K.-L. Chan, Science **358**, 1155 (2017)

[28] M. Qin, C.M. Chung, H. Shi, E. Vitali, C. Hubig, U. Schollwöck, S.R. White, and S. Zhang, Phys. Rev. X **10**, 031016 (2020)

[29] H.-C. Jiang and T.P. Devereaux, Science **365**, 1424 (2019)

[30] F. Simkovic, R. Rossi, and M. Ferrero, Phys. Rev. Res. **4** 043201 (2022)

[31] B. Xiao, Y.-Y. He, A. Georges, and S. Zhang, Phys. Rev. X **13**, 011007 (2023)

[32] H.Q. Lin and J.E. Hirsch, Phys. Rev. B **35**, 3359 (1987)

[33] W. Hofstetter and D. Vollhardt, Ann. Phys. (Berlin) **510**, 48 (1998)

[34] E. Langmann and M. Wallin, J. Stat. Phys. **127**, 825 (2007)

[35] N.D. Mermin and H. Wagner, Phys. Rev. Lett. **17**, 1133 (1966)

[36] M.S. Scheurer, S. Chatterjee, W. Wu, M. Ferrero, A. Georges, and S. Sachdev, Proc. Natl. Acad. Sci. USA **115**, E3665 (2018)

[37] S. Sachdev, Rep. Prog. Phys. **82**, 014001 (2019)

[38] P.M. Bonetti and W. Metzner, Phys. Rev. B **106**, 205152 (2022)

[39] R. Scholle, P.M. Bonetti, D. Vilardi, and W. Metzner, Phys. Rev. B **108**, 035139 (2023)

[40] R. Scholle, W. Metzner, D. Vilardi, and P.M. Bonetti, Phys. Rev. B **109**, 235149 (2024)

[41] S. Sachdev, H.D. Scammell, M.S. Scheurer, and G. Tarnopolsky, Phys. Rev. B **99**, 054516 (2019)

[42] O. Zachar, S.A. Kivelson, and V.J. Emery, Phys. Rev. B **57**, 1422 (1998)

[43] P.M. Bonetti and W. Metzner, Phys. Rev. B **105**, 134426 (2022)

[44] G. Baym and L.P. Kadanoff, Phys. Rev. **124**, 287 (1961)

[45] J.W. Negele and H. Orland: *Quantum Many-Particle Systems* (Addison-Wesley, 1987)

[46] Z.Y. Weng, C.S. Ting, and T.K. Lee, Phys. Rev. B **43**, 3790 (1991)

[47] H. Schulz, in D. Baeriswyl (ed.): *The Hubbard Model* (Plenum, New York, 1995)

[48] K. Borejsza and N. Dupuis, Phys. Rev. B **69**, 085119 (2004)

[49] Y. Zhang, E. Demler, and S. Sachdev, Phys. Rev. B **66**, 094501 (2002)

[50] M. De Prato, A. Pelissetto, and E. Vicari, Phys. Rev. B **74**, 144507 (2006)

[51] W. Metzner, M. Salmhofer, C. Honerkamp, V. Meden, and K. Schönhammer, Rev. Mod. Phys. **84**, 299 (2012)

[52] J. Wang, A. Eberlein, and W. Metzner, Phys. Rev. B **89**, 121116 (2014)

[53] R. Scholle, P.M. Bonetti, W. Metzner, and D. Vilardi, arXiv:2602.20073